

Arrested Kondo effect and hidden order in URu₂Si₂

Kristjan Haule and Gabriel Kotliar¹

¹Center for Materials Theory, Serin Physics Laboratory, Rutgers University,
136 Frelinghuysen Road, Piscataway, New Jersey 08854, USA.

PACS numbers: 71.27.+a, 72.15.Rn, 71.30.+h

Complex electronic matter exhibit subtle forms of self organization which are almost invisible to the available experimental tools, but which have dramatic physical consequences. One prominent example is provided by the actinide based heavy fermion material URu₂Si₂. At high temperature, the U-5*f* electrons in URu₂Si₂ carry a very large entropy. This entropy is released at 17.5 K via a second order phase transition [1] to a state which remains shrouded in mystery, and which was termed a "hidden order" state [2]. Here we develop a first principles theoretical method to analyze the electronic spectrum of correlated materials as a function of the position inside the unit cell of the crystal, and use it to identify the low energy excitations of the URu₂Si₂. We identify the order parameter of the hidden order state, and show that it is intimately connected with magnetism. We present first principles results for the temperature evolution of the electronic states of the material. At temperature below 70 K U-5*f* electrons undergo a multichannel Kondo effect, which is arrested at low temperature by the crystal field splitting. At lower temperatures, two broken symmetry states emerge, characterized by a complex order parameter ψ . A real ψ describes the hidden order phase, and an imaginary ψ corresponds to the large moment antiferromagnetic phase, thus providing a unified picture of the two broken symmetry phases, which are realized in this material.

URu₂Si₂ crystallizes in the body centered tetragonal structure displayed in Fig. 1A. Starting from a localized point of view for U-5*f* electrons, i.e., treating them as core states in density functional theory calculations, one obtains a set of wide bands, entirely of *spd* character, as shown in Fig. 1B. In an itinerant picture, there are *f* states close to the Fermi level which hybridize with the *spd* bands to form itinerant states of predominantly *f* character, with a bandwidth of the order of 1 eV. This is shown in Fig. 1C. This situation is realized in Ce and Yr based heavy fermion materials, whose electronic states are well described by narrowing the bands of the density functional theory by a factor of 10-1000, to account for the heavy mass [3].

For URu₂Si₂, we propose a new scenario for the transfer of atomic *f* weight to the itinerant carriers which

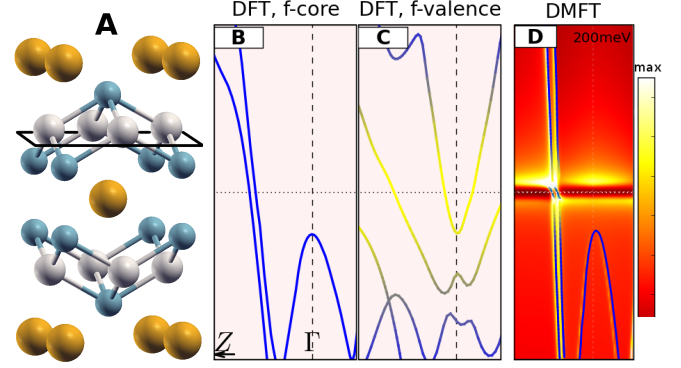


FIG. 1: (A) Crystal structure of URu₂Si₂. Gold, grey and green spheres correspond to U, Ru, and Si, respectively. The black box marks the cut of the unit cell for which we show electronic states in Fig. 2. (B,C,D) A sketch of the arrested Kondo effect phenomena. In the vertical axis we display the energy (in the interval $[-200 \text{ meV}, 200 \text{ meV}]$) and in the horizontal axis the momentum (around the center of the Brillouin zone). The horizontal dotted line marks the Fermi level. The light *spd* bands are plotted by blue lines, while the bright colors correspond to the primarily U-*f* spectra. In standard band structure calculation, the heavy *U* bands are either excluded from the calculation (shown in B), or included in the one electron theory (C). The many body calculation (D) shows the new phenomena of Kondo effect developing only at intermediate energy scales and intermediate temperatures $\Delta \lesssim T \lesssim T^*$, where $\Delta \sim 35 \text{ K}$ is the crystal field splitting and $T^* \sim 70 \text{ K}$ is the coherence scale. The temperature in panel (D) is $T = 19 \text{ K} < \Delta$ and color coding of the spectra is the projection of the total DMFT electronic spectra to the U-5*f* character. The DMFT method predicts the U 5*f* occupation to be 2.0, hence U-5*f* configuration in solid is U^{4+} .

we dub the "arrested Kondo effect". At high temperatures, above the characteristic coherence temperature $T^* \sim 70 \text{ K}$, the U-5*f* electrons are localized, and do not participate in forming the low energy bands. The *U* atoms settle in $5f^2$ configuration, for which the crystal environment chooses the non-degenerate atomic ground state. However, the first excited state, which is also non-degenerate, is only $\Delta = 35 \text{ K}$ above the ground state, as first observed in polarized neutron scattering experiments [4]. Hence in the temperature range $\Delta < T < T^*$, the ground state seems doubly degenerate, hence the Kondo effect develops, leading to formation of very narrow states near the Fermi energy, and a narrow peak in the density of states. The Kondo effect is partially arrested below

$T < \Delta$, because the crystal fields splitting between the two singlet states induces a partial gapping at the Fermi level. The situation is shown in Fig. 1C. A non-dispersing slab of f spectral weight is pushed to roughly 8 meV away from the Fermi energy. While only a small fraction of the f spectral weight is present at the Fermi level, it has a significant effect, resulting in a mass enhancement factor which is over 200 at $T = 19$ K. For temperatures above the crystal field splitting energy, $T \sim \Delta$, the electronic scattering rate is anomalously large. This is a signature of multichannel Kondo physics, whereby the two singlets play the role of the spin in the Kondo problem that scatters degenerate bands. The relevance of the two channel Kondo physics to U based impurity models was first proposed by D. Cox [5]. Indeed experimental data on dilute $U_x\text{Th}_{1-x}\text{Ru}_2\text{Si}_2$ systems are well described by the two channel Kondo model [6]. It is remarkable that the Fermi liquid regime in URu_2Si_2 can never be reached. Once the two channel Kondo effect is arrested by the crystal field splitting, long range order, driven by intersite effects, preempts the formation of a Fermi liquid state with a low coherent scale.

The one electron spectral function $A(\mathbf{r}, \omega)$ represents the quantum mechanical probability for adding or removing an electron with energy ω at a point \mathbf{r} in real space. We calculate it using the combination of the density functional theory and dynamical mean field theory (DMFT) [7]

$$A(\mathbf{r}, \omega) = \sum_{\mathbf{k}} \chi_{\mathbf{k}\alpha}^*(\mathbf{r}) [G_{\mathbf{k},\alpha\beta}(\omega) - G_{\mathbf{k},\beta\alpha}^*(\omega)] \chi_{\mathbf{k}\beta}(\mathbf{r}) \quad (1)$$

where $\chi_{\alpha}(\mathbf{r})$ are the basis functions, and $G_{\alpha\beta}$ is the electron Green's function expressed in the basis of χ . More details of the implementation of the DMFT method for this problem is given in the online material.

These computational studies are the theoretical counterpart of the scanning tunneling spectroscopy technique, that has been very useful in describing the properties of numerous correlated materials [8] and was very recently applied to URu_2Si_2 [9].

The evolution of the electron spectral function $A(\mathbf{r}, \omega)$ along the cut above U atom in the unit cell, as depicted in Fig. 1A, is displayed in Fig. 2. The curves have an asymmetric lineshape of the type

$$A(\omega) \propto [(q^2 - 1) + 2q(\omega/\Gamma)] / [(\omega/\Gamma)^2 + 1]$$

where Γ is the width, and q measures the asymmetry of the lineshape. These curves were first introduced by Fano [10], to describe scattering interference between a discrete state and a degenerate continuum of states. The continuum of states in scanning tunneling microscopy on URu_2Si_2 is provided by itinerant spd bands, and the narrow discrete states are the U -5 f electronic states, depicted with bright colors in Fig. 1D. Notice that the lineshape has the most characteristic Fano shape when the

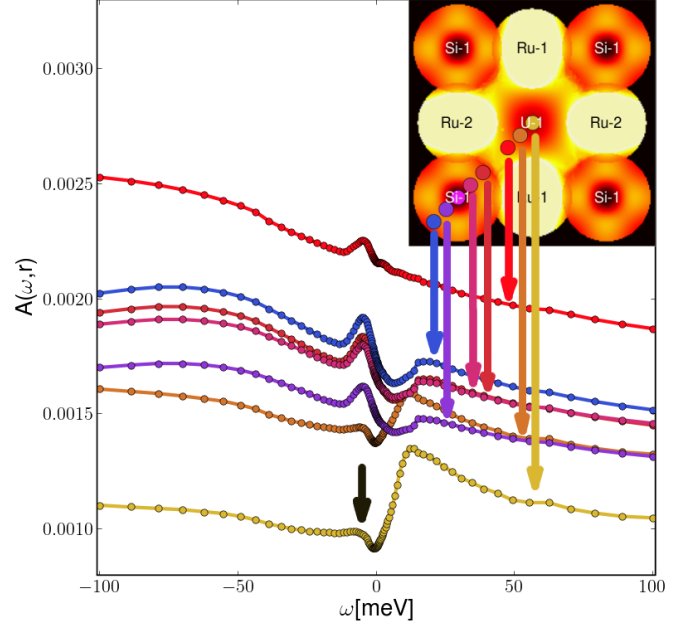


FIG. 2: (inset) The calculated electronic density $A(\mathbf{r}, \omega = 0)$ in real space at 20 K, as measured by scanning tunneling microscopy experiments. We take a representative cut in real space, sketched in Fig. 1, which cuts the U muffin-tin sphere at 3/4 height, guaranteeing a large matrix elements with the valence 4 f -electrons on U -atom. The main panel shows the energy dependence of the electronic density of states at various positions in real space. For each colored dot we show a curve in the main panel, which has the same color as the dot.

position \mathbf{r} is on the U or Si atom, with positive asymmetry $q > 0$ on U atom and negative asymmetry $q < 0$ on Si atom. With the exception of the small peak, marked with black arrow in Fig. 2, the lineshape on U atom can be well fitted to the Fano lineshape with parameter $q = 1.24$ and $\Gamma = 6.82$ meV.

The main features of our calculations, including the characteristic lineshape, the width, and the strength of the asymmetry of the Fano lineshape, as well as the additional small peak around 6 meV, were recently measured in scanning tunneling experiments by J.C. Seamus Davis group [9], the first experiment of this type on a heavy fermion system.

To understand the origin of the small peak at 6.8 meV, we integrate the spectra over the whole unit cell and resolve it in the different angular momentum channels of the different atoms. This orbitally resolved spectra at low energies is shown in Fig. 3A.

While there are plenty of Si -3 p and Ru -4 d state at the Fermi level, these states are only weakly energy dependent in 300 meV interval. On the other hand, the heavy U -5 f electron states have a dip and a peak at the

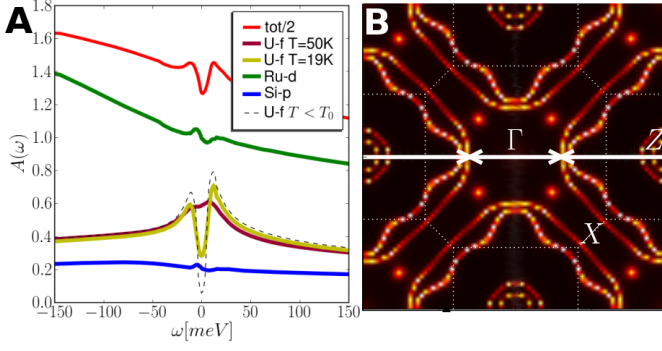


FIG. 3: **(A)** The total density of electronic state (red) and the orbitally resolved components at $T = 19\text{ K}$. Also shown is the U - f component at higher $T = 50\text{ K}$. Using Fermi liquid estimate for the specific heat coefficient $\gamma \propto A(\omega = 0)/Z$ we obtain $\gamma \sim 85\text{ mJ}/(\text{mol K}^2)$ at $T = 50\text{ K}$ ($1/Z \sim 60$) and $\gamma \sim 140\text{ mJ}/(\text{mol K}^2)$ at $T = 19\text{ K}$ ($1/Z \sim 200$). **(B)** The DMFT Fermi surface of URu_2Si_2 in the paramagnetic state $T = 20\text{ K} > T_{\text{order}}$. We take a two dimensional horizontal cut in the the tetragonal body centered Brillouin zone passing through the origin.

same energy of 6.8 meV , which is clearly visible in the real space spectra in Fig. 2. Therefore it is the U - $5f$ non-lorentzian shape of the electronic density of state, which is responsible for the additional peak and the asymmetry variation in the unit cell. This dip-peak lineshape is also the key to unravelling the puzzle of the electronic structure of the material, since it shows that instead of a regular lorentzian Kondo resonance, we have a double peak at low temperature, with a pseudogap at zero energy. This is the signature of the Kondo effect, loosing its strength at temperature T below the crystal field splitting energy $T < \Delta$. Below the ordering temperature (the ordering will be discussed below), the pseudogap in the partial U - $5f$ spectra is considerably enhanced, as presented in Fig. 3A. Note that due to mixing of spd and f states, there is finite admixture of U - $5f$ state at the Fermi level, giving some "heaviness" to the quasiparticle even below the ordering temperature.

The electronic states can also be resolved in momentum space by computing the spectral function $A(\mathbf{k}, \omega)$. The active state at the Fermi level, given by peaks of $A(\mathbf{k}, \omega = 0)$, determine the Fermi surface of the material, which is displayed in Fig. 3B.

For many Ce based heavy fermion compounds, the Fermi surface of itinerant DFT calculation, as well as DMFT calculation, accounts for the experimentally measured de-Hass van Alphen frequencies. On the other hand, the DMFT Fermi surface of URu_2Si_2 , shown in Fig. 3B, is qualitatively similar to the localized DFT calculation, with $5f$'s excluded from the valence bands [11]. Note that the Luttinger's theorem, which counts the number of electrons modulo 2, does not constraint

the Fermi surface of the material. Hence the Fermi surface does not need to resemble the itinerant DFT result.

The first principles DMFT calculations demonstrate that for URu_2Si_2 the $5f^2$ configuration has the dominant weight. This has important consequences, since it allows the physical Fermi surface to have the same volume as the system with no f electrons, such as ThRu_2Si_2 [12].

Finally, the DMFT Fermi surface is hole-like, and the large hole Fermi surface centered at Z displays characteristic wave vectors $(0.6, 0, 0)a^*$ and $(1.4, 0, 0)a^*$ shown in Fig. 3B. Recent neutron scattering experiments display low energy spectral weight at these incommensurate wave vectors [13, 14, 15].

In the long range order phase, the Fermi surface substantially reconstructs, and multiple small electron and hole pockets appear, making this system a compensated metal, with the same number of hole and electron carriers.

The U - $5f^2$ configuration has the total angular momentum $J = 4$ and is split into five singlets and two doublets in the tetragonal crystal environment of URu_2Si_2 . The relative energy of these crystal field levels is still an open problem and several sequences have been proposed. For a recent review see Ref. [16].

The wave functions of the U - $5f^2$ configuration, with the largest weight in the DMFT density matrix, are

$$|\emptyset\rangle = \frac{i}{\sqrt{2}}(|4\rangle - |-4\rangle) \quad (2)$$

$$|1\rangle = \frac{\cos(\phi)}{\sqrt{2}}(|4\rangle + |-4\rangle) - \sin(\phi)|0\rangle \quad (3)$$

Here $|J_z\rangle = |J = 4, J_z\rangle$ is a two particle state of the $J = 4$ multiplet. We obtained $\phi \sim 0.23\pi$. The separation between the two singlets is of the order of 35 K . The probability for the atomic ground state, $|\emptyset\rangle$, and the first excited state, $|1\rangle$, at 20 K is 0.54 and 0.1 , respectively.

The transition into ordered states requires an understanding of the collective excitations, which are bound states of particle hole pairs. The identification of the low lying singlets leads us to consider the following order parameter for URu_2Si_2

$$\psi_i = \langle X_{\emptyset 1}(\mathbf{R}_i) \rangle \quad (4)$$

where $X_{\emptyset 1} = |\emptyset\rangle\langle 1|$ is the Hubbard operator which measures the excitonic mixing between the two lowest lying U - $5f$ singlets at lattice site \mathbf{R}_i .

This order parameter is complex. Its real part is proportional to the hexadecapole operator of A_{2g} irreducible representation of the tetragonal symmetry, $\text{Re}\psi \propto \langle (J_x J_y + J_y J_x)(J_x^2 - J_y^2) \rangle$, introduced in the context of nuclear physics long ago. Its imaginary part is proportional to the magnetization along the z axis, $\text{Im}\psi \propto \langle J_z \rangle$, which is the only direction allowed within this crystal field set of states. Experimentally, the moment indeed points in z direction [4].

At low temperatures, we found two different stable DMFT solutions, describing ordered states with non zero staggered $\langle\psi\rangle$ with wave vector $\mathbf{Q} = (0, 0, 1)$. The first solution has $\langle\psi\rangle$ purely real and describes the hidden order phase of URu₂Si₂. This solution has zero magnetic moment, does not break time reversal symmetry and has nonzero hexadecapole. The second DMFT solution, has a purely imaginary $\langle\psi\rangle$ and we associate this phase with the large moment antiferromagnet phase, which is experimentally realized at pressures larger than 0.7 GPa [17, 18, 19, 20]. Hence, the microscopic approach succeeds in unifying two very distinct broken symmetry states in a single complex order parameter. The existence of a solutions with either purely real or purely imaginary ψ , but without mixtures, indicates a first order phase transition between these two phases, as observed in the pressure experiments of Ref. [17, 18, 19, 20].

It is useful to visualize the meaning of this order parameter in a limiting case of a simple atomic wavefunction, where it takes the form $|gs\rangle = \cos(\theta)|\emptyset\rangle + \sin(\theta)e^{i\varphi}|1\rangle$. The average magnetic moment of the ground state is hence $\langle gs|\mathbf{J}|gs\rangle = 4\cos(\phi)\sin(2\theta)\sin(\varphi)*(0, 0, 1)$. If $\varphi = \pi/2$, we have a phase with large magnetic moment, and if φ vanishes, the moment vanishes.

Our theory provides a natural explanation for a large number of experiments, which are very puzzling, when examined from other perspectives and suggests new experiments.

Firstly, it has been advocated phenomenologically that even though the hidden order phase and the large moment phase have distinct order parameters, the behavior of many observables across the transition is remarkably similar. The term *adiabatic continuity* has been used to describe this situation [17, 21], but it is not justified on the theoretical grounds since the two phases are separated by a first order phase transition. The proposed order parameter ψ_i , which unifies the no-moment and large moment phase, explains why even though the two phases are separated by a first order phase transition, they are in many respects very similar, for example in the critical temperature, and entropy change across the transition.

Secondly, at the hidden order transition, a small gap of the order of 10 meV opens in the 5f quasiparticle spectra, as seen in optical conductivity [22], specific heat [23], thermal conductivity [24], and relaxation rate measurements [25, 26]. On the other hand the dc resistivity continues to decrease at low temperatures [27], since it is dominated by the itinerant *spd* carriers. This fact is hard to understand in a simple itinerant density wave picture. The *f* states gap at low energies is also seen in neutron scattering experiments [4, 14, 15].

Thirdly, unlike density functional theory calculations [28], our approach described a strongly correlated normal state with large entropy, and can account for large specific heat coefficient in the paramagnetic state of the material.

It has recently been proposed that one can detect hexadecapole order using resonant X-ray technique [30]. This would be a direct test of our proposed order parameter. A high resolution angle resolved photoemission spectroscopy can detect the small kink in the very low energy spectra (< 10 meV) of Fig. 1D, which is a unique signature of the arrested Kondo effect. It would be interesting to control the crystal field splitting energy Δ . A slight decrease (increase) of Δ , will increase (decrease) the hidden order transition temperature.

Finally, our results set the stage for understanding the mysterious superconducting transition that takes place at the much lower temperatures ($T_c = 0.8$ K). Hidden order is fertile ground for superconductivity, while the large moment antiferromagnetic phase completely eliminates this instability. Our results suggest that Cooper pairing can take place only when the electrons propagate in the time reversal symmetric background, but unravelling the precise origin of the superconductivity in this material will require further sleuthing.

-
- [1] Palstra, T.T.M. *et al.* Superconducting and magnetic transitions in the heavy fermion system URu₂Si₂. *Phys. Rev. Lett.* **55**, 2727 (1985).
 - [2] Tripathi, V., Chandra, P., and Coleman, P. Sleuthing hidden order. *Nature Physics*, **3**, 78 (2007).
 - [3] Allen, J.W. The Kondo Resonance in Electron Spectroscopy. *J. Phys. Soc. Japan* **74**, 34-48 (2005).
 - [4] Broholm, C., *et al.* Magnetic Excitations and Ordering in the Heavy-Electron Superconductor URu₂Si₂. *Phys. Rev. Lett.* **58**, 1467 (1987).
 - [5] Cox, D.L. Kondo effect in real metals. *Phys. Rev. Lett.* **59**, 1240 (1987).
 - [6] Amitsuka, H., and Sakakibara, T. Single Uranium Site Properties of the Dilute Heavy Electron System $U_xTh_{1-x}Ru_2Si_2$. *J. Phys. Soc. Jpn.*, **63**, 736 (1994).
 - [7] Kotliar, G. *et al.* Electronic structure calculations with dynamical mean-field theory. *Rev. Mod. Phys.* **78**, 865 (2006).
 - [8] Kohsaka, Y. *et al.* Investigation of the vanishing pattern of Cooper pairs in Bi₂Sr₂CaCu₂O₈, approaching the Mott insulator. *Nature* **454**, 1072 (2008).
 - [9] Schmidt, A., Hamidian, M., Meier, F., Wahl, P., Haenke, T., Balatsky, A.V., Luke, G., and Davis J.C. Visualizing Heavy Fermion Formation within the Kondo Lattice of URu₂Si₂. *Abstract number: BAPS.2009.MAR.V29.3, APS March Meeting, Pittsburgh, 2009.*
 - [10] Fano, U. Effects of Configuration Interaction on Intensities and Phase Shifts. *Phys. Rev.* **124**, 1866 (1961).
 - [11] Denlinger, J.D. *et al.* Temperature Dependent 5f states in URu₂Si₂. *J. Electron Spectrosc. Relat. Phenom.* **117-118**, 347 (2001).
 - [12] Denlinger, J.D. *et al.* k-space Fingerprinting of U Valence in URu₂Si₂. *Abstract number: BAPS.2009.MAR.Q2.2, APS March Meeting, Pittsburgh, 2009.*
 - [13] Broholm, C. *et al.* Magnetic excitations in heavy fermion superconductors. *Phys. Rev. B* **43**, 12809 (1991).
 - [14] Villaume, A. *et al.* Signature of hidden order in heavy

- fermion superconductor URu₂Si₂: Resonance at the wave vector $Q_0 = (1, 0, 0)$. *Phys. Rev. B* **78**, 012504 (2008).
- [15] Wiebe, C.R. *et al.* Gapped itinerant spin excitations account for missing entropy in the hidden-order state of URu₂Si₂. *Nature Physics* **3**, 96, (2007).
- [16] Kiss, A., and Fazekas, P., Group theory and octupolar order in URu₂Si₂. *Phys. Rev. B* **71**, 054415 (2005).
- [17] Pfleiderer, C., Mydosh, J.A., and Vojta, M. Pressure dependence of the magnetization of URu₂Si₂. *Phys. Rev. B* **74**, 104412 (2006).
- [18] Amitsuka, H. *et al.* Pressure-temperature phase diagram of the heavy-electron superconductor URu₂Si₂. *J. Magn. Magn. Mat.* **310**, 214, (2007).
- [19] Motoyama, G. *et al.* Electrical Resistivity and Thermal Expansion Measurements of URu₂Si₂ under Pressure. *J. Phys. Soc. Jpn.* **77**, 123710 (2008).
- [20] Hassinger, E. *et al.* Temperature-pressure phase diagram of URu₂Si₂ from resistivity measurements and calorimetry: Hidden order and Fermi-surface nesting. *Phys. Rev. B* **77**, 115117 (2008).
- [21] Jo, Y.J. *et al.* Field-Induced Fermi Surface Reconstruction and Adiabatic Continuity between Antiferromagnetism and the Hidden-Order State in URu₂Si₂. *Phys. Rev. Lett.* **98**, 166404 (2007).
- [22] Bonn, D.A., Garret, J.D., and Timusk, T. Far infrared properties of URu₂Si₂. *Phys. Rev. Lett.* **61**, 1305 (1988).
- [23] van Dijk, N.H. *et al.* Specific heat of heavy-fermion URu₂Si₂ in high magnetic fields. *Phys. Rev. B* **56**, 14493 (1997).
- [24] Behnia, K. *et al.* Thermal Transport in the Hidden-Order State of URu₂Si₂. *Phys. Rev. Lett.* **94**, 156405 (2005).
- [25] Matsuda, K. *et al.* Spatially Inhomogeneous Development of Antiferromagnetism in URu₂Si₂: Evidence from ²⁹Si NMR under Pressure. *Phys. Rev. Lett.* **87**, 087203 (2001).
- [26] Maple, M.B. *et al.* Partially Gapped Fermi Surface in the Heavy-Electron Superconductor URu₂Si₂. *Phys. Rev. Lett.* **56**, 185 (1986).
- [27] Schoenes, J. *et al.* Hall-effect and resistivity study of the heavy-fermion system URu₂Si₂. *Phys. Rev. B* **35**, 5375 (1987).
- [28] Elgazzar, S. *et al.* Uncovering the hidden order in URu₂Si₂: Identification of Fermi surface instability and gapping. *Nature Materials*, published online 22 Feb 2009, doi: 10.1038/nmat2395.
- [29] Yokoyama, M. *et al.* Competition between hidden order and antiferromagnetism in URu₂Si₂ under uniaxial stress studied by neutron scattering. *Phys. Rev. B* **72**, 214419 (2005).
- [30] Kuramoto, Y., Kusunose, H., Kiss, A. Diffraction from ordered states of higher multipoles. *Physica B: Condensed Matter*, **383**, 5 (2006).

ACKNOWLEDGEMENTS

We are grateful to J. Allen and J. Denlinger for fruitful discussion. K.H was supported by Grant NSF NFS DMR-0746395 and Alfred P. Sloan fellowship. G.K. was supported by NSF DMR-0906943.

ONLINE MATERIAL: ARRESTED KONDO EFFECT AND HIDDEN ORDER IN URu₂Si₂

The details of the method

We carried out the band structure calculation for URu₂Si₂ using recently developed method which combines the Density Functional Theory (DFT) and Dynamical Mean Field Theory (DMFT). The combination DFT+DMFT (for a review see Ref. [1]) contains some aspects of band theory, adding a “frequency-dependent local potential” to the Kohn-Sham Hamiltonian. It also contains some aspects of quantum chemistry, carrying out an exact local configuration interaction procedure by summing all local Feynman diagrams. The details of the current implementation of the method are given in Ref. [2] (see in particular Eqs.(2) and (25) that give the site resolved tunneling spectra).

The crystal structure of URu₂Si₂ is body-centred tetragonal with point group I4/mmm (ThCr₂Si₂ type). The lattice parameters are $a = 4.1240 \text{ \AA}$, $c = 9.5566 \text{ \AA}$ and the internal parameter $z = 0.3727$ [3].

The on-site screened Coulomb repulsion in actinides ranges between 4 – 5 eV. For uranium, which is on itinerant side of actinides, our estimate for U is 4.0 eV. The Slater integrals were computed by atomic physics program of R.D. Cowan [4], and scaled by 70% to account for screening in the solid. Their values are $F_2 = 6.81 \text{ eV}$, $F_4 = 4.55 \text{ eV}$, $F_6 = 3.36 \text{ eV}$.

For the double-counting, we used the standard, localized formula $E_{DC} = U(n_{imp} - 1/2) - J(n_{imp}/2 - 1/2)$ with $J = F_2/11.92196532 = 0.57 \text{ eV}$, and n_{imp} is the average number of electrons in the U-5*f* orbital, for URu₂Si₂ $n_{imp} \approx 2$.

We used two complementary impurity solvers, the One Crossing Approximation (OCA) [1, 2] and the Continuous Time Quantum Monte Carlo (CTQMC) [5]. The first is implemented directly on the real axis and is of invaluable help to analytically continue the exact Monte Carlo imaginary time data. For the DFT part, we used the LMTO method of S. Savrasov [6] and we crosschecked results with LAPW method, as implemented in Wien2K [7].

The URu₂Si₂ compound is one of the rare cases, where the charge self-consistency of DFT+DMFT is crucial. Namely, the DFT potential needs to be computed on the self-consistent DFT+DMFT electronic charge. The non-self consistent version of DFT+DMFT severely misplaces the important low energy bands.

The broken symmetry states

At low temperature, we succeeded to stabilize two broken symmetry states with the ordering wave vector $Q = (0, 0, 1)$: An antiferromagnetic state with large magnetic moment, and a broken symmetry state with no magnetic moment.

There are two independent ways to look at the nature of the broken symmetry state: i) An atomic perspective, which was given in the main text of the article. The broken symmetry solution is associated with the local order parameter $\psi = \langle X_{\emptyset 1} \rangle = \langle |\emptyset\rangle\langle 1| \rangle$, where $X_{\emptyset 1}$ is the Hubbard operator, which mixes two crystal field singlet states, the ground state and the first excited state of the atom. The two atomic states are given by

$$|\emptyset\rangle = \frac{i}{\sqrt{2}}(|4\rangle - |-4\rangle) \quad (5)$$

$$|1\rangle = \frac{\cos(\phi)}{\sqrt{2}}(|4\rangle + |-4\rangle) - \sin(\phi)|0\rangle. \quad (6)$$

Here atomic states $|0\rangle$ and $|4\rangle$ correspond to the $|J = 4, J_z = 0\rangle$ and $|J = 4, J_z = 4\rangle$, respectively. ii) Alternatively, one can examine the structure of Green's function, the central object of the DFT+DMFT method. To understand the symmetry of the broken symmetry solution, one can examine the equal time analog, which is the density matrix of the problem.

Below we will derive the connection between the density matrix of the problem and the atomic eigenstates for the case of URu₂Si₂. We first evaluate the projection of the density matrix operator $f_{\alpha}^{\dagger}f_{\beta}$ to the atomic eigenstates. It is useful to view the broken symmetry from the point of view of the Green's functions matrix and its equal time limit (the density matrix). Exact diagonalization of the atomic problem leads to the following relations

$$f_{5/2}^{\dagger}f_{-3/2} = -a|4\rangle\langle 0| + b|0\rangle\langle -4| + \dots \quad (7)$$

$$f_{-3/2}^{\dagger}f_{5/2} = -a|0\rangle\langle 4| + b|-4\rangle\langle 0| + \dots \quad (8)$$

$$f_{3/2}^{\dagger}f_{-5/2} = b|4\rangle\langle 0| - a|0\rangle\langle -4| + \dots \quad (9)$$

$$f_{-5/2}^{\dagger}f_{3/2} = b|0\rangle\langle 4| - a|-4\rangle\langle 0| + \dots \quad (10)$$

$$f_{-5/2}^{\dagger}f_{-5/2} = c_1|-4\rangle\langle -4| + c_2|0\rangle\langle 0| + \dots \quad (11)$$

$$f_{-3/2}^{\dagger}f_{-3/2} = c_3|-4\rangle\langle -4| + c_4|0\rangle\langle 0| + \dots \quad (12)$$

$$f_{3/2}^{\dagger}f_{3/2} = c_3|4\rangle\langle 4| + c_4|0\rangle\langle 0| + \dots \quad (13)$$

$$f_{5/2}^{\dagger}f_{5/2} = c_1|4\rangle\langle 4| + c_2|0\rangle\langle 0| + \dots \quad (14)$$

with $a \approx 0.77$, $b \approx 0.25$, $c_1 \approx 0.97$, $c_2 \approx 0.07$, $c_3 \approx 0.98$, $c_4 \approx 0.63$.

The relation between the crystal field atomic eigenstates ($|\emptyset\rangle$, $|1\rangle$, $|2\rangle$) and the direct atomic states $|J, J_z\rangle$ ($J_z = 4, -4, 0$) is

$$\begin{bmatrix} |\emptyset\rangle \\ |1\rangle \\ |2\rangle \end{bmatrix} = \begin{bmatrix} \frac{i}{\sqrt{2}} & \frac{-i}{\sqrt{2}} & 0 \\ \frac{\cos \Phi}{\sqrt{2}} & \frac{\cos \Phi}{\sqrt{2}} & -\sin \Phi \\ \frac{\sin \Phi}{\sqrt{2}} & \frac{\sin \Phi}{\sqrt{2}} & \cos \Phi \end{bmatrix} \begin{bmatrix} |4\rangle \\ |-4\rangle \\ |0\rangle \end{bmatrix}. \quad (15)$$

Inverting this matrix equation and inserting it into Eqns. (7)-(14), we obtain the following form of the density matrix

$$\langle f_{5/2}^\dagger f_{-3/2} \rangle = \frac{i \sin \Phi}{\sqrt{2}} (b\psi^* - a\psi) + \dots = \frac{\sin \Phi}{\sqrt{2}} [i(b-a)\text{Re}\psi + (b+a)\text{Im}\psi] + \dots \quad (16)$$

$$\langle f_{-3/2}^\dagger f_{5/2} \rangle = \frac{i \sin \Phi}{\sqrt{2}} (a\psi^* - b\psi) + \dots = \frac{\sin \Phi}{\sqrt{2}} [-i(b-a)\text{Re}\psi + (b+a)\text{Im}\psi] + \dots \quad (17)$$

$$\langle f_{3/2}^\dagger f_{-5/2} \rangle = \frac{-i \sin \Phi}{\sqrt{2}} (a\psi^* - b\psi) + \dots = \frac{\sin \Phi}{\sqrt{2}} [i(b-a)\text{Re}\psi - (b+a)\text{Im}\psi] + \dots \quad (18)$$

$$\langle f_{-5/2}^\dagger f_{3/2} \rangle = \frac{-i \sin \Phi}{\sqrt{2}} (b\psi^* - a\psi) + \dots = \frac{\sin \Phi}{\sqrt{2}} [-i(b-a)\text{Re}\psi - (b+a)\text{Im}\psi] + \dots \quad (19)$$

$$\langle f_{-5/2}^\dagger f_{-5/2} \rangle = \frac{-ic_1 \cos \Phi}{2} (\psi^* - \psi) + \dots = -c_1 \cos \Phi \text{Im}\psi + \dots \quad (20)$$

$$\langle f_{-3/2}^\dagger f_{-3/2} \rangle = \frac{-ic_3 \cos \Phi}{2} (\psi^* - \psi) + \dots = -c_3 \cos \Phi \text{Im}\psi + \dots \quad (21)$$

$$\langle f_{3/2}^\dagger f_{3/2} \rangle = \frac{ic_3 \cos \Phi}{2} (\psi^* - \psi) + \dots = c_3 \cos \Phi \text{Im}\psi + \dots \quad (22)$$

$$\langle f_{5/2}^\dagger f_{5/2} \rangle = \frac{ic_1 \cos \Phi}{2} (\psi^* - \psi) + \dots = c_1 \cos \Phi \text{Im}\psi + \dots \quad (23)$$

where ψ is the order parameter $\psi = \langle |\emptyset \rangle \langle 1| \rangle$. Here the dots (\dots) stand for the projection to the other atomic states, the part of the projection which is nonzero in the paramagnetic state.

Setting $\text{Im}\psi = 0$ and $\text{Re}\psi \neq 0$, we see that $\delta \langle f_{5/2}^\dagger f_{-3/2} \rangle = -\delta \langle f_{-3/2}^\dagger f_{5/2} \rangle$ and $\delta \langle f_{-5/2, -5/2}^\dagger f_{-5/2, -5/2} \rangle = \delta \langle f_{5/2, 5/2}^\dagger f_{5/2, 5/2} \rangle$. The symbol δ stands for the change of the density matrix compared to its value in the paramagnetic state. The structure of the Green's function in the hidden-order phase is therefore

$$\Delta = \left(\begin{array}{c|cccccc} & -5/2 & -3/2 & -1/2 & 1/2 & 3/2 & 5/2 \\ \hline -5/2 & \Delta_A & 0 & 0 & 0 & \Delta_\epsilon + \Delta_\alpha & 0 \\ -3/2 & 0 & \Delta_B & 0 & 0 & 0 & \Delta_\epsilon + \Delta_\beta \\ -1/2 & 0 & 0 & \Delta_C & 0 & 0 & 0 \\ 1/2 & 0 & 0 & 0 & \Delta_C & 0 & 0 \\ 3/2 & \Delta_\epsilon - \Delta_\alpha & 0 & 0 & 0 & \Delta_B & 0 \\ 5/2 & 0 & \Delta_\epsilon - \Delta_\beta & 0 & 0 & 0 & \Delta_A \end{array} \right) \quad (24)$$

Here Δ_ϵ is the off-diagonal term, present also in the paramagnetic phase and comes due to the tetragonal crystal environment. Since the magnetic moment of this state vanishes ($\langle \mathbf{J} \rangle = 0$), we associate this moment-free phase with the hidden order state.

The second solution has $\text{Im}\psi \neq 0$ and $\text{Re}\psi = 0$, hence $\delta \langle f_{5/2}^\dagger f_{-3/2} \rangle = \delta \langle f_{-3/2}^\dagger f_{5/2} \rangle$ and $\delta \langle f_{-5/2, -5/2}^\dagger f_{-5/2, -5/2} \rangle \neq \delta \langle f_{5/2, 5/2}^\dagger f_{5/2, 5/2} \rangle$. The structure of the Green's function in the local moment antiferromagnetic phase is therefore given by

$$\Delta = \left(\begin{array}{c|cccccc} & -5/2 & -3/2 & -1/2 & 1/2 & 3/2 & 5/2 \\ \hline -5/2 & \Delta_A & 0 & 0 & 0 & \Delta_\epsilon & 0 \\ -3/2 & 0 & \Delta_B & 0 & 0 & 0 & \Delta'_\epsilon \\ -1/2 & 0 & 0 & \Delta_C & 0 & 0 & 0 \\ 1/2 & 0 & 0 & 0 & \Delta'_C & 0 & 0 \\ 3/2 & \Delta_\epsilon & 0 & 0 & 0 & \Delta'_B & 0 \\ 5/2 & 0 & \Delta'_\epsilon & 0 & 0 & 0 & \Delta'_A \end{array} \right) \quad (25)$$

with $\Delta_A \neq \Delta'_A$, $\Delta_B \neq \Delta'_B$, $\Delta_C \neq \Delta'_C$. This phase has nonzero magnetic moment $\langle \emptyset | J | \emptyset \rangle = 4$ and hence we associate it with the large moment antiferromagnetic phase in URu₂Si₂.

Another way to look at the broken symmetry state is by using the perturbation theory around the atomic limit. In the expansion with respect to the hybridization strength Δ (between the atom and the conduction bands), the leading term of the Lutting-Ward functional contains the following terms

$$\Phi = \sum_m c_m G_{mm}^* [G_{01} * (\Delta_{-5/2, 3/2} - \Delta_{3/2, -5/2}) + G_{10} * (\Delta_{-3/2, 5/2} - \Delta_{5/2, -3/2})] + \sum_m d_m G_{mm}^* (G_{01} - G_{10}) * (\Delta_{j_z} - \Delta_{-j_z}) \quad (26)$$

Here the pseudoparticle Green's function G_{01} and G_{10} are connected to the Hubbard operators by $G_{01}(\tau - \tau') = -\langle T_\tau X_{01}(\tau) X_{01}(\tau') \rangle$ and $G_{01}(\tau - \tau') = -\langle T_\tau X_{10}(\tau) X_{10}(\tau') \rangle$, respectively.

One possible self-consistent solution of this functional is $G_{01} = G_{10} \neq 0$, $(\Delta_{-5/2,3/2} - \Delta_{3/2,-5/2}) = (\Delta_{-3/2,5/2} - \Delta_{5/2,-3/2}) \neq 0$ and $\Delta_{j_z} = \Delta_{-j_z}$. This solution corresponds to moment-free phase.

The second possible solution is $G_{01} = -G_{10} \neq 0$, $\Delta_{j_z} \neq \Delta_{-j_z}$ and $\Delta_{-5/2,3/2} = \Delta_{3/2,-5/2}$, $\Delta_{-3/2,5/2} = \Delta_{5/2,-3/2}$, which corresponds the antiferromagnetic solution.

-
- [1] G. Kotliar, S. Y. Savrasov, K. Haule, V. S. Oudovenko, O. Parcollet, and C. A. Marianetti Rev. Mod. Phys. **78**, 865 (2006).
 - [2] Kristjan Haule, Chuck-Hou Yee, Kyoo Kim, arXiv:0907.0195.
 - [3] A.P. Ramires, T. Siegrist, T.T.M. Palstra, J.D. Garrett, E. Bruck, A.A. Menovsky, J.A. Mydosh, Phys. Rev. B **44**, 5392 (1991).
 - [4] R. D. Cowan, *The Theory of Atomic Structure and Spectra* (Univ. California Press, Berkeley, 1981).
 - [5] Kristjan Haule, Phys. Rev. B **75**, 155113 (2007).
 - [6] S. Y. Savrasov, Phys. Rev. B **54**, 16470 (1996).
 - [7] P. Blaha, K. Schwarz, G. K. H. Madsen, K. Kvasnicka, and J. Luitz, Wien2K (Karlheinz Schwarz, Technische Universitat Wien, Austria, 2001).
-